Proceedings of ASME Turbo Expo 2011
GT2011
June 6-10, 2011, Vancouver, British Columbia, Canada

GT2011-45822

Geometry Optimization of Textured 3-D Micro- Thrust Bearings

C.I. Papadopoulos
School of Naval Architecture and Marine Engineering,
National Technical University of Athens,
15710 Zografos, Greece

E.E. Efstathiou
School of Naval Architecture and Marine Engineering,
National Technical University of Athens,
15710 Zografos, Greece

P.G. Nikolakopoulos
Machine Design Laboratory,
Department of Mechanical Engineering and Aeronautics,
University of Patras, 26504 Patras, Greece

L. Kaiktsis
School of Naval Architecture and Marine Engineering,
National Technical University of Athens,
15710 Zografos, Greece

ABSTRACT

The paper presents an optimization study of the geometry of three-dimensional micro-thrust bearings, in a wide range of convergence ratios. The optimization goal is the maximization of the bearing load carrying capacity. The bearings are modeled as micro-channels, consisting of a smooth moving wall (rotor), and a stationary wall (stator) with partial periodic rectangular texturing. The flow field is calculated from the numerical solution of the Navier-Stokes equations for incompressible isothermal flow; processing of the results yields the bearing load capacity and friction coefficient. The geometry of the textured channel is defined parametrically for several width-to-length ratios. Optimal texturing geometries are obtained by utilizing an optimization tool based on genetic algorithms, which is coupled to the CFD code. Here, the design variables define the bearing geometry and convergence ratio. To minimize the computational cost, a multi-objective approach is proposed, consisting in the simultaneous maximization of the load carrying capacity and minimization of the bearing convergence ratio. The optimal solutions, identified based on the concept of Pareto dominance, are equivalent to those of single-objective optimization problems at different convergence ratio values. The present results demonstrate that the characteristics of the optimal texturing patterns depend strongly on both the convergence ratio and the width-to-length ratio. Further, the optimal load carrying capacity increases at increasing convergence ratio, up to an optimal value, identified by the optimization procedure. Finally, proper surface texturing provides substantial load carrying capacity even for parallel or slightly diverging bearings. Based on the present results, we propose simple formulas for the design of textured micro-thrust bearings.

Keywords: 3-D micro-thrust bearings, rectangular texturing, multi-objective optimization, Navier-Stokes equations.

INTRODUCTION

Efficient and reliable bearing systems are essential for micro-rotating machinery, such as micro-motors and micro-turbines [1-3]. In micro- thrust bearing applications, liquid lubricants provide increased rotor stability, and reduce the probability of solid contact between rotating and stationary parts. The technology of future tribological contact systems will depend on the environmental policies adopted; as lower pollution and energy consumption will be demanded, materials and tribosystems should preferably be light, and characterized by low friction, minimal wear, and high load capacity. Based on recent research, textured slider bearings appear as promising candidates for meeting the above expectations.

Recent technological advances in surface treatment methods, such as micro-stereolithography, chemical etching, surface indentation, micromachining, LIGA processes and laser ablation, have enabled the implementation of artificial texture patterns in machine components, with resolution accuracy of a few microns or even less [4], both for journal and thrust bearings. In bearing applications, major performance indices are the load carrying capacity and the friction coefficient. Several studies utilizing the Reynolds equation demonstrate that texture patterns (irregularities in the bearing surface) have beneficial effects on the performance of bearing configurations, in particular thrust bearings [5-10].

For textured infinite-width sliders, the applicability of the Reynolds equation has been investigated in [11]. It was shown that the validity of the Reynolds equation cannot be decided by the Reynolds number alone, as the dimple geometric parameters may have an equally important influence. For infinite- and finite-width slider bearings, CFD studies have been utilized to calculate the flow field and the resulting load and friction forces, for a number of texture patterns [12-15].

First optimization studies of surface texturing are reported in [16-18], utilizing the Reynolds equation. In [16], a PDE-constrained optimization solver has been used to maximize load carrying capacity, while in [17] sensitivity analysis and genetic algorithms have been used to minimize the friction coefficient of slider bearings with rectangular dimples. In [18], finite-width bearings with different rectangular and trapezoidal texture patterns have been investigated, and the effects of cavitation analysed. In [19], the optimization of trapezoidal texture patterns of two-dimensional (infinitely wide) sliders was considered, by coupling an optimization approach with CFD simulations. It was concluded that, for parallel and converging sliders, proper texturing results in substantial load capacity levels. One of the conclusions reported in [19] is that, in comparison to rectangular texture patterns, the benefits from the introduction of trapezoidal texture geometries are marginal.

In three-dimensional (finite-width) bearings, side leakage is expected to affect the flow structure and pressure distribution, and thus alter the optimal texture patterns of two-dimensional (infinitely wide) bearings. Thus, following the work reported in [19], in the present study the more realistic three-dimensional slider geometries are considered, with the goal of identifying optimal texture patterns of rectangular shape, for maximum load carrying capacity. To define the slider geometry, a parametric CAD model is generated, which can account for different bearing width-to-length ratios, and roughness geometries of rectangular shape. The model is utilized by a Navier-Stokes solver. To minimize the total computational cost, a multi-objective optimization approach is proposed, in which the bearing convergence ratio is utilized both as a design variable and an objective function. Here, parallel, converging and diverging bearing geometries are all considered. Results are obtained by coupling the CFD code with an optimization tool based on genetic algorithms. Optimal solutions are identified using the concept of Pareto dominance, and are physically interpreted. The present study thus aims at identifying optimal rectangular texture geometries for different bearing width-to-length and convergence ratios, at quantifying their performance potential, and at relating optimization results to flow physics.

The paper is organized as follows: The problem definition and computational approach are first presented, with a short reference to the optimization procedure. Optimization results are then presented and discussed, and, finally, the main findings are summarized.

PROBLEM DEFINITION

Micro- thrust bearing geometry

The geometry of a water-lubricated three-dimensional converging micro- thrust bearing with partial periodic rectangular texturing is presented in Figure 1. The fluid convects towards the outlet, and builds up pressure, which exerts forces on the bearing walls. Pressure buildup is due to the presence of rectangular dimples, extending in the spanwise direction over the bearing width, and (possibly) also due to the converging geometry. Force equilibrium is attained by the presence of an external vertical load W on both walls. Energy is expended by the work done by the shear forces at the moving wall-fluid interface.

A three-dimensional parametric CAD model has been built, with geometry dimensions representative of micro-bearings. The bearing height changes from the inlet height H_1 (x=0) to its value H_0 at the outlet (x = L). H_0 and H_1 are controlled by the convergence ratio, $k = \left(H_1 - H_0\right)/H_0$. Evidently, zero values of k account for parallel sliders, while positive or negative values of k correspond to converging or diverging sliders, respectively. The value of minimum film thickness, H_{min}, depends on the sign of k ($H_{min}=H_0$ for $k \geq 0$; $H_{min}=H_1$ for $k<0$). In the present study, H_{min} is assumed in all cases constant, equal to 0.05 mm. The length L of the bearing is controlled by the non-dimensional parameter $l = L/H_{\min}$; here l is equal to 100. The bearing width, B, is controlled by the ratio B/L.

Part of the stationary wall is textured with rectangular dimples (Figure 1). For all cases, an untextured part (sill) at the inlet, of length equal to 1/100 of the total length, i.e. $l_{ui} = 0.01$, is considered. The untextured length at the bearing outlet is variable, controlled by the non-dimensional parameter l_{uo} . The textured part exhibits N periodic texture cells. Each texture cell is defined by the cell length, L_c, the dimple length, L_d, and the dimple depth, H_d, see Figure 1(b). These dimensional geometric parameters are controlled by the texture density, ρ_T , and the relative dimple depth, s .

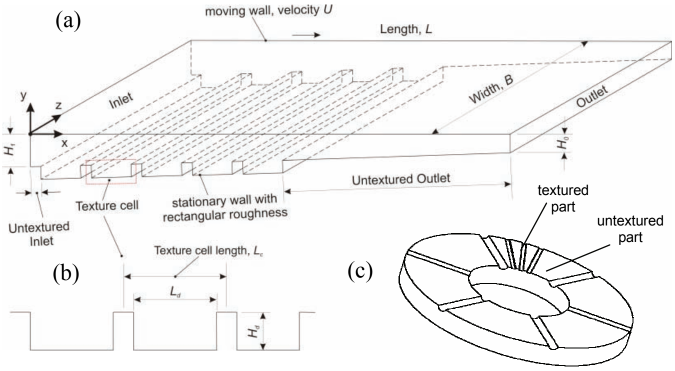

Figure 1. (a) Three-dimensional textured converging slider geometry (parallel slider for $H_1=H_0$, diverging slider for $H_1<H_0$). (b) Geometry of dimples. (c) Typical thrust bearing application with partial texturing.

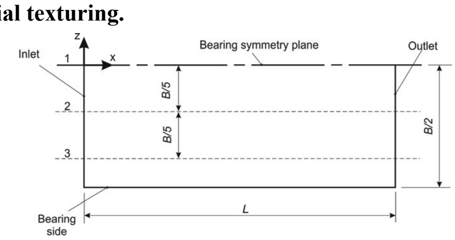

Figure 2. Half-slider top view, in which three x-y cross sections are indicated.

Governing equations and assumptions

The flow is considered isothermal, and the minimum pressure value is assumed to be above the vapor pressure; thus, cavitation is not accounted for. The conservation equations for unsteady incompressible and isothermal flow, with zero gravitational and other external body forces, are:

Mass conservation equation

$$\nabla \cdot \mathbf{V} = 0 \tag{1}$$

Momentum equations

$$\frac{\partial \mathbf{V}}{\partial t} + \mathbf{V} \cdot \nabla \mathbf{V} = -\frac{1}{\rho}\nabla p + \frac{\mu}{\rho}\nabla^2 \mathbf{V} \tag{2}$$

Equations (1) and (2) are solved with the CFD code ANSYS CFX. From dimensional analysis, it follows that, for given geometry, the flow dynamics depends on the Reynolds number, Re, defined here in terms of the moving wall velocity and the minimum film thickness, H_{min}. Geometry optimization is performed for Re=1, a value representative of micro-bearing applications, while the effect of Reynolds number on bearing performance is also considered. In the present dimensional model, a value of Re=1 corresponds to a wall velocity $U = 0.01785 \text{ m s}^{-1}$, and values of the fluid thermophysical properties equal to those of water at 25 ^{o}C, see [19]. Results are presented in non-dimensional form.

Spatial discretization, boundary and initial conditions

As the steady low Reynolds number flow is symmetric about the channel mid-plane, only half of the channel is modeled, to reduce computational cost (see Figure 2). Typical 3-D meshes generated consist of approximately 300,000 hexahedral finite volumes. The corresponding finite volume size at a x-y cross-section of the slider is $0.04H_{min}$-$0.1H_{min}$, with a minimum of 15 cells in the untextured region, along the y-direction. The grid is denser in near-wall regions, see [19] for details on grid design. In the spanwise direction, discretization utilizes a typical finite volume size of approximately 1-$2H_{min}$. Spatial resolution tests have been performed by generating meshes with numbers of finite volumes both lower and substantially higher (approximately 1,000,000 finite volumes) than the typical meshes used. The relative differences in the flow integral quantities (load capacity and friction force) between typical and very fine meshes were in all cases on the order of 1%.

The bearing walls are considered impermeable. The bottom wall is stationary. The upper wall is assumed to be moving at a constant velocity U (parallel to the x axis), $u(x, y=0, z) = U$. No-slip conditions are assumed at both walls.

The inlet and outlet surfaces of the bearing, see Figures 1 and 2, are considered openings: the pressure is assumed constant, with the same value $p=0$ prescribed at both boundaries, while a Neumann boundary condition is assumed for the velocity. At the bearing side, $z=-B/2$, an outflow condition is prescribed, i.e., in addition to the above assumptions, $w \leq 0$. Symmetry boundary conditions are prescribed at the bearing symmetry plane, $z=0$: $w=0$, $\partial u/\partial z = \partial v/\partial z = 0$.

All simulations were initialized from zero velocity and pressure fields. For Re=1, the governing equations were integrated for a total time of 2×10^{-2} s, with a time step of 1×10^{-4} s. This integration time is about 7 times higher than the convection time scale of the problem, which, for Re=1, coincides with the diffusion time scale. Smaller time step values and longer integration times were used at higher Re values. In all cases, convergence to steady state was verified by monitoring the computed velocity and pressure at a number of representative points within the flow domain.

The shear (friction) force and the vertical force exerted to the rotor are calculated at steady state by integrating the shear stress, τ, and pressure, p, respectively, over the rotor surface:

$$F_{fr} = 2\int_{-B/2}^{0}\int_{0}^{L}\tau\, dxdz\ ,\quad F_p = 2\int_{-B/2}^{0}\int_{0}^{L} p\, dxdz = W \qquad (3)$$

The friction coefficient is defined as $f = F_{fr}/F_p$.

Validation of CFD results

The present CFD model was validated by comparing computational results against published literature data for two problems relevant to the present study. First, a similar flow problem in a 2-D converging textured bearing was solved, and the results compared against the literature data of [12]. This problem consists of a textured slider bearing exhibiting three rectangular dimples, as shown in Figure 3(a) (inset sketch). The bearing height at outlet, H_0, is 0.03 mm; the bearing non-dimensional length is l=200. The length of each dimple, L_d, is 0.3 mm, the dimple density, ρ_T, is equal to 0.429, whereas two different values of $s = H_d/H_{\min}$ are considered, namely 0.75 and 0.1. The Reynolds number is equal to 1. Figure 3(a) presents the distribution of computed pressure along the moving wall, as well as the results of [12], illustrating a very good agreement.

In a second step, calculations were performed for 3-D smooth converging sliders of various B/L and convergence ratio values, and processed for the load carrying capacity. In Figure 3(b), the results are compared against the published data of [20], illustrating a very good agreement.

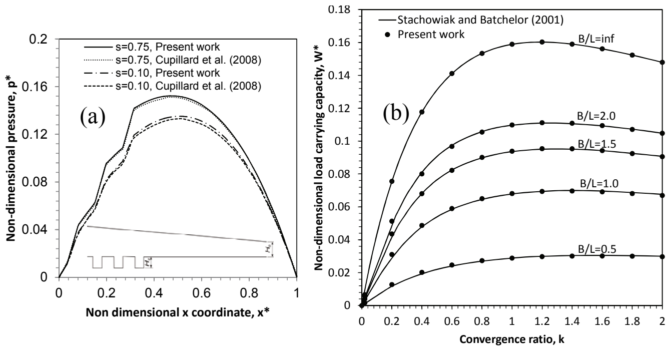

Figure 3. Validation of present CFD results against literature data: (a) Computed non-dimensional pressure distribution vs. non-dimensional streamwise coordinate for a converging micro-bearing with texturing. (b) Computed non-dimensional load carrying capacity vs. convergence ratio of smooth rectangular sliders, for a number of *B/L* ratios.

OPTIMIZATION OF SLIDER BEARING GEOMETRY

Problem formulation

The geometry of the slider is defined in terms of the design variables B/L, N, l_{uo}, s, ρ_T and k, defined in the Nomenclature. In [19], it has been shown that W^* is an increasing function of dimple density, ρ_T. However, a maximum value of ρ_T must be set due to strength limitations of the stator. In the present work a value of ρ_T equal to 0.83 is selected, which corresponds to a minimum distance between two consecutive dimples equal to 20% of the dimple length. As documented in several literature studies, see e.g. [9,19] and references therein, W^* is a decreasing function of the number of dimples, N. However, at lower values of N, the effects of wear on bearing performance are more pronounced. A representative value of N=5 is considered in the present optimization study. The effects of varying dimple density and dimple number on bearing performance are also investigated.

The goal of the present work is the optimization of texture geometry of slider bearings, for maximum load carrying capacity, W^*, over a wide range of convergence ratios. A straightforward (but computationally costly) approach would be to solve several single-objective optimization problems (each one corresponding to a different value of convergence ratio). As documented in [19], in textured sliders, W^* is an increasing function of convergence ratio, k, up to an optimal value. Using this property of textured converging sliders, we propose a multi-objective optimization procedure, and seek combinations of the non-dimensional variables l_{uo}, s, and k, which simultaneously maximize the load carrying capacity, and minimize the convergence ratio. We emphasize that here convergence ratio, k, is used both as an independent variable and as an objective function of the problem. This optimization concept, to our knowledge not utilized in previous literature studies, is equivalent to several single-objective optimization problems, each one aiming at maximizing W^* for a given convergence ratio value. The proposed formulation aims at minimizing the total computational cost, by evolving only one initial generation of randomly created individuals. A substantial reduction in computational cost is expected due to the fact that the evolution of geometry at a certain window of convergence ratios gains from the good properties of texture geometries at neighboring convergence ratio values. The present optimization problem may formally be expressed as follows:

For given width-to-length (B/L) ratio, find the optimum combination of the non-dimensional parameters l_{uo}*, s and k which simultaneously maximizes the non-dimensional load carrying capacity,* W^**, and minimizes convergence ratio, k.*

Thus, a different optimization problem is solved for each value of *B/L*; here, *B/L* takes values from the group $\{0.5,\ 1.0,\ 1.5,\ 2.0,\ \inf\}$, i.e. five different optimization problems are solved, spanning the range from low- to infinitely high width-to-length ratio bearings. Evidently, the case of *B/L*=inf corresponds to a 2-D flow problem. In all cases, the range of the design variables is prescribed as follows:

l_{uo} : Takes values in the range [0, 1]. For $l_{uo} = 0$, texturing evidently extends until the outlet of the bearing. A value of, say, $l_{uo} = 0.4$, corresponds to a stator texturing which extends from the inlet until 60% of the stator length.

s : Takes values in the range [0.1, 2]. The dimple depth H_d thus takes values in the range $0.1H_{min}$ to $2H_{min}$.

k : Takes values in the range [-0.4, 2]. Negative values of *k* correspond to diverging sliders. As evidence of positive pressure buildup even for slightly diverging textured sliders has been recently reported [19], diverging sliders are also considered here.

To illustrate the nature of the present approach, optimization results for the case of an infinitely wide slider are presented in Figure 4(b), in which the final Pareto front for the two-objective optimization problem is also shown. Each combination of the independent variables (l_{uo}, s, k) corresponds to a slider with different texture geometry and convergence ratio, and results in a load carrying capacity W^*. The aggregate of computed solutions for several values of the independent variables is represented by the cross symbols of Figure 4(b). The dashed line corresponds to the load carrying capacity of a smooth converging slider. Apparently, for a given value of *k*, there exist combinations of the texturing parameters l_{uo} and *s* which lead to improved slider performance, in comparison to that of a smooth slider, and other combinations that lead to deteriorated performance. Among the different possible bearing designs (combinations of the independent variables), there exist some for which the following hold: (a) a higher value of load carrying capacity cannot be achieved unless a higher value of convergence ratio is to be accepted, and (b) a lower value of convergence ratio cannot be achieved unless a lower value of load carrying capacity is to be accepted. These points are *non-dominated*, and lie on the Pareto front of the present optimization problem (Figure 4(b), solid line). Obviously, these points correspond to the maximum load carrying capacity that can be achieved at a given convergence ratio, by application of proper texturing at the slider stator. The right-most point of the Pareto front corresponds to the maximum value of W^* that the bearing can provide by application of proper texturing, at the optimal convergence value, k_{opt}. Thus, by evolving only one generation of randomly generated geometries (i.e., at a minimal computational cost), the methodology proposed in the present work gives both the optimal bearing geometry at different converge ratio values, as well as the geometry corresponding to the global optimum of load carrying capacity.

Optimization method

The final set of optimum solutions for the two-objective optimization problem is obtained by evolving, by means of a genetic algorithm, an initial randomly generated population (generation). The evolution produces subsequent generations, utilizing the operations of parent selection, cross-over and mutation (see [21] for a detailed discussion). In each generation, the collection of all non-dominated solutions is the *Pareto front*, identified by utilizing the concept of Pareto Ranking, see Figure 4(a,b). In the present work, geometry optimization is performed by coupling the CFD code with an optimization tool; the latter utilizes the ParadisEO genetic algorithms library [22], and adopts the Non-dominated Sorting Genetic Algorithm NSGA-II for Pareto ranking [23]. The entire procedure is presented schematically in Figure 4(c).

Optimization results

Figure 5 presents the obtained optimal load carrying capacity, W^*, versus convergence ratio, *k*, of textured sliders with different values of width to length ratio, *B/L*. The dashed lines with circles correspond to the final Pareto fronts (outcome of the optimization procedure). The solid lines correspond to computed W^* of smooth sliders as a function of convergence ratio. For each *B/L* value, a horizontal dashed line is plotted, corresponding to the (maximum) W^* of an optimal step bearing. Figure 6 illustrates the optimal micro-bearing geometries, for parallel sliders and sliders with convergence ratio $k=k_{opt}$. Based on Figure 5, the following observations can be made:

- The introduction of texturing substantially improves load carrying capacity, in comparison to smooth sliders. The improvement is drastic for small values of *k*.
- At their optimum configuration (right-most point of each Pareto front), textured sliders provide increased W^*, in comparison to smooth sliders of (a different) optimal *k*. The improvement is approximately 4% for small- to medium-width sliders, reaching 7.5% for sliders of infinite width.
- Parallel sliders (*k*=0) with optimal texturing provide substantial load carrying capacity. The optimal W^* value of textured parallel sliders with *B/L*=0.5 is 0.013, 41% of the maximum attainable W^* (right-most point of the corresponding Pareto front). The percentage increases almost linearly at increasing *B/L*, taking values of 53%, 59%, 63% and 72% for sliders with *B/L* values of 1.0, 1.5, 2.0 and inf, respectively.
- Substantial pressure buildup is possible even for slightly diverging textured channels. For very wide sliders, pressure buildup is possible even for values of *k* lower than -0.4.
- The optimal value k_{opt} (corresponding to the right-most point of each Pareto front) is a decreasing function of *B/L*, taking the minimum value of 0.75 at *B/L*=inf.
- For small values of *B/L* (approximately up to 1.0), optimized textured sliders provide higher load carrying capacity than optimal step bearings of the same *B/L*.

A comparison of the above performance characteristics to other types of thrust bearings is of interest. Efficient thrust bearings suitable for micro-scale applications include herringbone and spiral groove bearings. Based on the present results, optimal textured sliders with *B/L* ratios higher than approximately 2.0 provide increased non-dimensional load carrying capacity, in comparison to optimal herringbone bearings; for a performance superior to that of spiral groove bearings, wider textured sliders (with *B/L* larger than approximately 3.0) are necessary [24]. However, herringbone and spiral groove bearings require higher fabrication accuracy, while their performance is more sensitive to fabrication errors and wear. Further, both herringbone and spiral groove bearings provide decreased damping, affecting rotor stability performance.

For the textured bearings of the present study, the optimal combinations of the non-dimensional geometric parameters l_{uo} and *s* of slider bearings are presented in Figure 7(a-j) as a function of convergence ratio, k. These combinations correspond to the points forming the Pareto fronts of Figure 5. A least squares fitting method is used to fit a straight line through each set of points, and the corresponding line equation is presented in each graph. The intercept of each line equation is the optimal parameter value of a parallel textured slider (k=0); the (positive or negative) slope represents the dependence on convergence ratio.

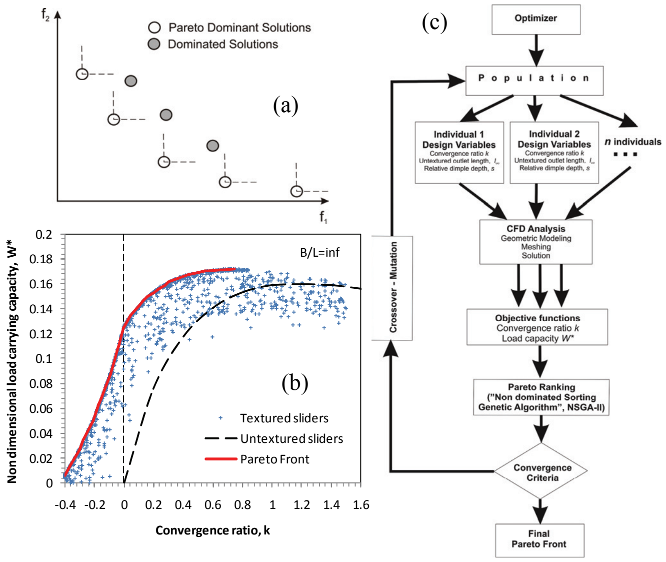

Figure 4. (a) Sketch of Pareto front concept for a minimization problem with two objective functions. (b) Non-dimensional load carrying capacity vs. convergence ratio for infinite width untextured and textured sliders, and corresponding Pareto front. (c) Optimization flow chart of the present study.

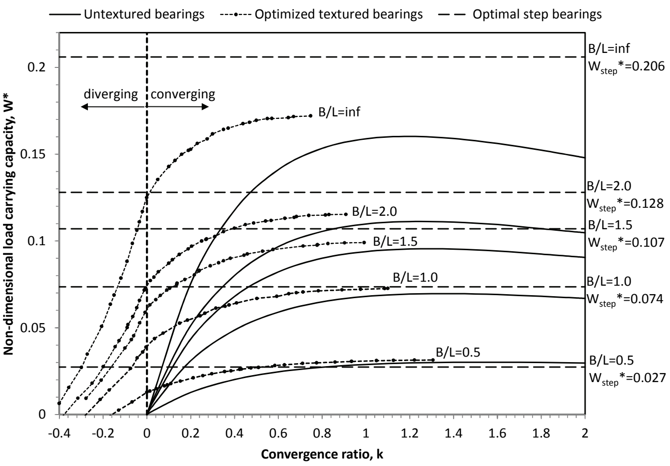

Figure 5. Optimal non-dimensional load carrying capacity, W^*, versus convergence ratio, k, for textured sliders of different B/L ratios. Results for smooth converging channels and optimal step bearings are also presented.

Figure 7(a-e) shows that, for parallel sliders, the optimal value of l_{uo} decreases at increasing B/L, obtaining the minimum value of 0.364 for infinitely wide sliders. Further, the curve slope is positive for small B/L values (increased untextured length at increasing k), and becomes negative for large values of B/L. The trend is physically plausible, since, for small B/L values, larger textured parts would allow for increased side leakage of fluid, thus decreasing the pressure integral (load carrying capacity). On the other hand, for large values of B/L, side leakage is less pronounced, therefore, larger textured parts are favored, which contributes to pressure buildup.

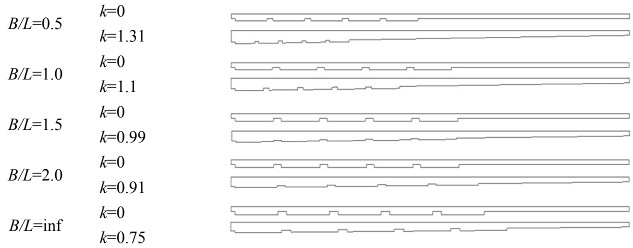

Figure 6. Optimal micro-bearing geometries for various B/L ratios. Cases of k=0 and k=k_{opt} are presented. (Domain is compressed by a factor of 33% in the x direction.)

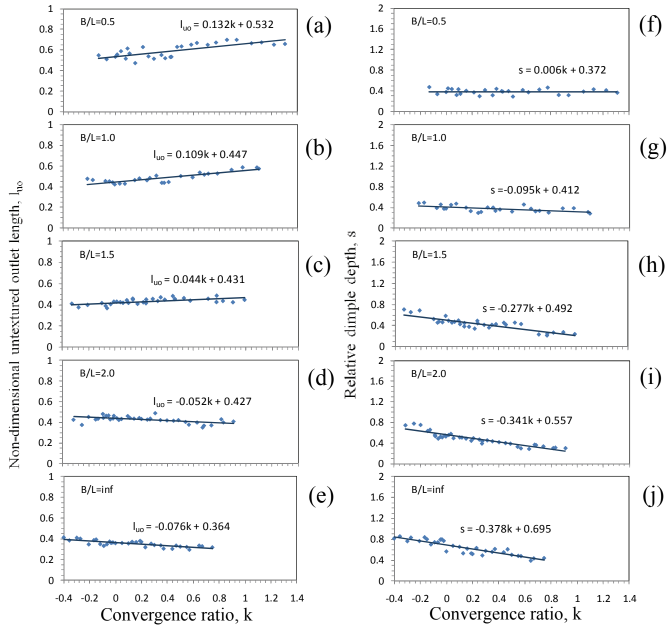

Figure 7. Optimal values of l_{uo} and s versus k, for different values of B/L. Line fits to the computed data are also included.

Regarding the relative dimple depth, s, Figure 7(f-j) illustrates that, for parallel sliders, the optimal s increases at increasing B/L, taking the maximum value of 0.695 for B/L=inf. For short sliders (B/L=0.5), the s over k slope is nearly zero, i.e., optimal dimple depth is practically independent of k. For bearings with higher values of B/L, the slope is negative, i.e., smaller dimple depths are favored at increasing values of k. It is known that, in textured bearings, increase of dimple height leads to increased pressure gradient in the streamwise direction, up to a certain dimple height at which backflow is initiated [19]. On the other hand, side leakage (therefore, increased pressure drop) is more pronounced in the case of large dimple heights, especially for small values of B/L. Further, as k increases, pressure buildup is due to both the dimple effect and the wedge effect of the converging surfaces. The contribution of dimples in pressure buildup is thus dominant for small k values, but becomes less important for steeper sliders. Thus, an optimum value of dimple depth exists for every combination of B/L and k, which is identified by the optimization process.

Next, the sensitivity of the principal objective function, W^*, to the design variables in the regime of the optimum is investigated. Here, the case of B/L equal to 2.0 at the optimum value of k (right-most point of the corresponding Pareto front of Figure 5) is considered. Each of the three independent geometric parameters of the present study (l_{uo}, s and k) is varied around its optimal value; the others are kept constant. The effect on W^* is illustrated in Figure 8. Clearly, for all variables, any change in their values results in decreased W^*, which illustrates that the algorithm has indeed converged to a local maximum. The results of Figure 8 illustrate that the untextured outlet length, l_{uo}, affects most the solution, followed by the relative dimple depth, s. Computational results for other B/L values (not shown, for brevity) demonstrate the same trends.

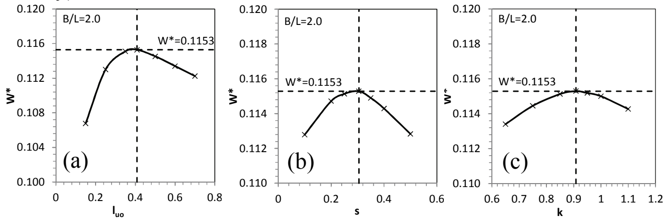

Figure 8. Optimal bearings with B/L=2.0: variation of load carrying capacity versus the design variables, in the regime of the optimum.

Next, the dependence of flow characteristics on the design variables is discussed for the cases of infinite width sliders, as well as for sliders with B/L equal to 2.0. Figure 9(a-b) presents the (non-dimensional) pressure distribution on the moving wall of an infinite parallel slider, for different values of l_{uo} and s, in the regime of the optimum. It is observed that longer untextured lengths increase the pressure buildup slope, see Figure 9(a); however, pressure buildup is maintained over a shorter distance, which results in reduced levels of the maximum pressure. On the other hand, smaller untextured lengths (equivalently: longer dimples) allow for pressure buildup over a longer extent. In the latter case, the pressure buildup slope is however lower, contributing to a decrease of the maximum pressure. Apparently an optimum value of untextured length exists in between, which is identified by the optimization process. Further, it is observed that either increase or decrease of relative dimple depth, s, around the optimum leads to decreased pressure buildup slope, see Figure 9(b). As analyzed in [19], values of s smaller than the optimum one lead to decreased second derivative of the streamwise velocity profile in the dimpled areas (therefore, decreased pressure buildup slope). For values of s larger than the optimum, a recirculation zone in the dimpled area occurs, also resulting in a milder pressure buildup.

Figure 9(c-d) presents similar results for a converging slider of infinite width. Here, k is equal to the optimum value of 0.75. In this case, pressure buildup is due to both the effect of dimples and the wedge effect of the converging surfaces. As deduced from Figure 9(c-d), the trends are similar to those in parallel sliders. However, the dependence of W^* on l_{uo} and s is less pronounced, due to the dominant contribution of the wedge effect in pressure buildup.

Figure 10(a-c) presents the distribution of non-dimensional pressure, p^*, at the moving wall of a parallel slider (k=0) with B/L=2, for different values of non-dimensional untextured outlet length, l_{uo}, at and around the optimum. Further, Figure 10(d-f) presents the corresponding distribution of p^* at three cross-sections of the moving wall; the location of these cross-sections is illustrated in Figure 2. Pressure is maximum at the bearing mid-plane (cross-section 1), decreasing towards the side edges of the bearing (cross-sections 2, 3), due to fluid leakage. Other observations are similar to those of an infinite width parallel bearing. In particular, longer untextured lengths increase the pressure buildup slope, see Figure 10(d-f), however, pressure buildup is maintained over a shorter extent, and thus lower levels of maximum pressure are attained. On the other hand, shorter untextured lengths allow for pressure buildup over a longer extent, but with a lower pressure buildup slope. Further, the existence of longer dimpled area leads to increased fluid leakage at the bearing sides, increasing the corresponding pressure drop (see Figure 10(a), and 12(f) for l_{uo}=0.3). Load carrying capacity, being the surface integral of pressure, thus decreases. The optimum value of untextured length is identified by the optimization process.

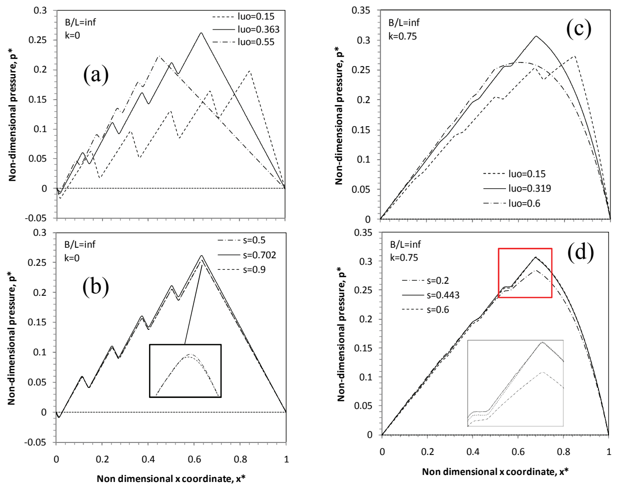

Figure 9. B/L=inf: distributions of non-dimensional pressure on the moving wall of the slider, for different values of non-dimensional untextured outlet length, l_{uo}, and relative dimple height, s. Graphs (a) and (b) correspond to parallel sliders (k=0). Graphs (c) and (d) correspond to convergent sliders of k=k_{opt}. The solid lines correspond to optimal points of the Pareto front.

Figure 11(a-f) presents pressure distributions for different values of relative dimple depth, s, at and around the optimum. It is observed that increase or decrease of s around the optimum leads to decreased pressure buildup slope, due to effects analyzed for the case of an infinitely wide slider. In addition, in finite-width sliders, an increase of dimple depth contributes to increased fluid leakage at the bearing sides, increasing the corresponding pressure drop (see Figure 11(c), and 11(f) for s=0.7).

In the case of converging finite-width sliders, pressure buildup is more complex. Figure 12(a-c) presents plots of non-dimensional pressure at the moving wall of a converging slider of k=k_{opt}=0.91, with B/L=2.0, for values of non-dimensional untextured outlet length, l_{uo}, at and around the optimum. Figure 12(d-f) presents the corresponding pressure distribution at the three cross-sections of Figure 2. In the case of longer untextured lengths, the pressure buildup slope is slightly increased, see Figure 12(d-f), however, pressure buildup is maintained over a shorter length, therefore lower levels of maximum pressure are attained. On the other hand, smaller untextured lengths allow for pressure buildup over a longer extent, leading to a larger value of maximum pressure, affecting mostly the bearing area near the outlet. However, the increased length of dimples leads to an increased pressure drop at the sides of the bearing. Evidently, optimum load carrying capacity is attained at a value of l_{uo} for which the gain due to increased maximum pressure balances the pressure decrease in the near-side region. This value is identified by the optimization process.

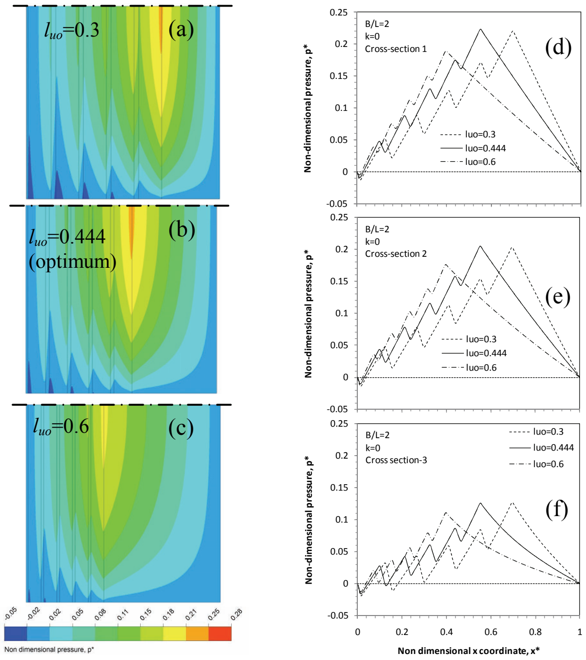

Figure 10. *B/L*=2.0, *k*=0: (a)-(c) Color-coded contours of non-dimensional pressure on the moving wall of the slider, for different values of non-dimensional untextured outlet length, l_{uo}. (d)-(f) Corresponding distribution of non-dimensional pressure at three cross-sections of the moving wall, depicted in Figure 2.

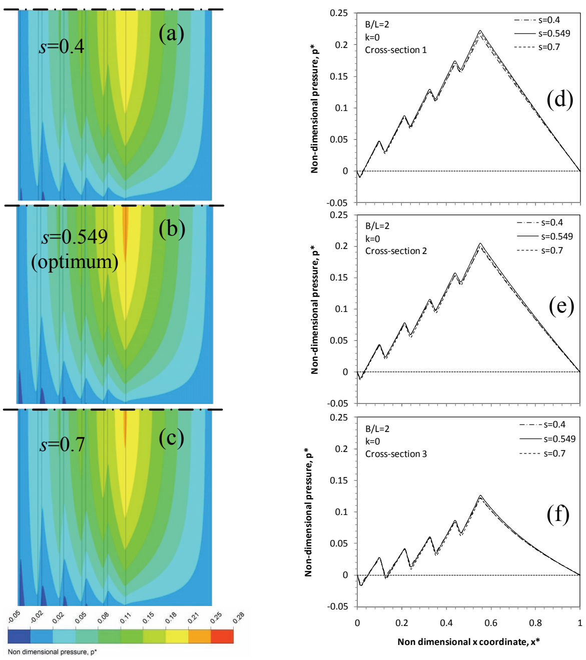

Figure 11. *B/L*=2.0, *k*=0: (a)-(c) Color-coded contours of non-dimensional pressure on the moving wall of the slider for different values of relative dimple height, *s*. (d)-(f) Corresponding distribution of non-dimensional pressure at three cross-sections of the moving wall, depicted in Figure 2.

For sliders with *B/L* values lower than 2.0, the observations are similar to those of the case *B/L*=2.0, analyzed above. In general, in low-width sliders, the effects of pressure drop in the side regions are more pronounced, which favors convergence to optimum geometries with lower dimple depth and shorter textured length.

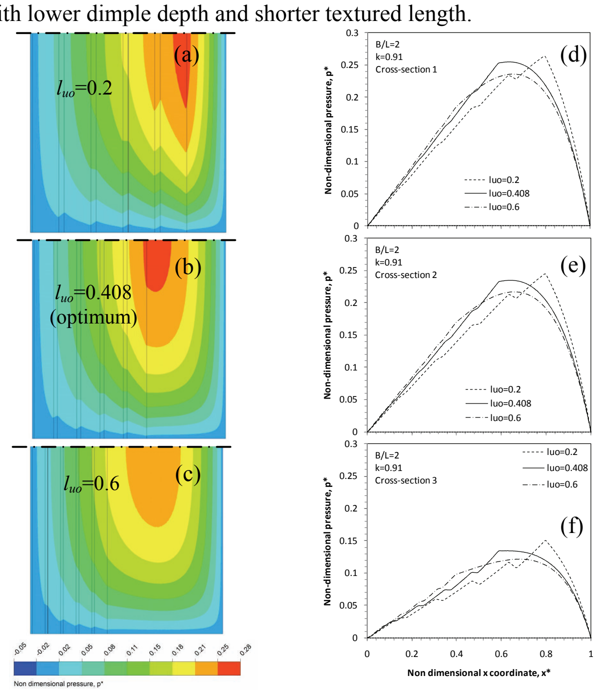

Figure 12. *B/L*=2.0, *k*=0.91: (a)-(c) Color-coded contours of non-dimensional pressure on the moving wall of the slider, for different values of non-dimensional untextured outlet length, l_{uo}; (d)-(f) Corresponding distribution of non-dimensional pressure at three cross-sections of the moving wall, depicted in Figure 2.

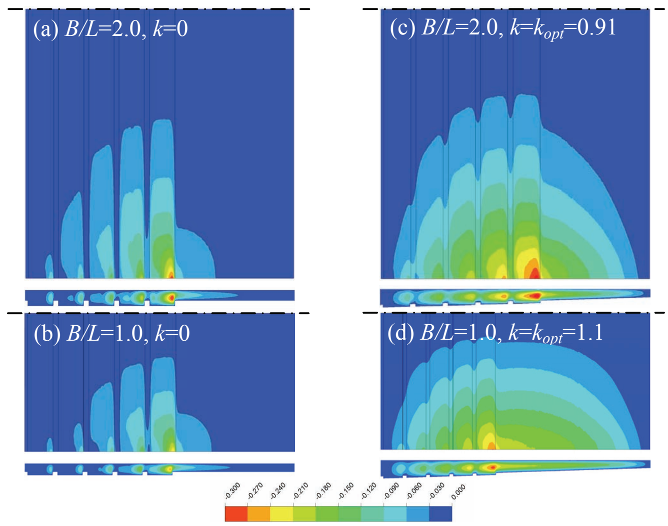

Figure 13. Color-coded contours of non-dimensional w-velocity, at a x-z plane located at y=-0.8H_{min} and at the x-y plane corresponding to the bearing side (*z*=-*B*/2), for: (a) *B/L*=2.0, *k*=0, (b) *B/L*=1.0, *k*=0, (c) *B/L*=2.0, *k*=0.91, and (d) *B/L*=1.0, *k*=1.1. (In the x-y plane, domain is compressed by a factor of 3 in the x direction.)

Figure 13(a-d) presents distributions of the spanwise velocity component at a representative plane of constant y-coordinate, as well as at the bearing side plane. Here, two values of *B/L* are considered, equal to 2.0 and 1.0, while the texture patterns are those obtained for optimal parallel bearings (k=0), and those of the global optimum. In parallel bearings, as pressure build-up is only due to the presence of dimples, side leakage is almost exclusively present in the dimpled regime. Pressure build-up is also due to the wedge effect in converging bearings, and thus non-negligible side leakage is present in the untextured outlet region, as well as in the gaps between consecutive dimples. In all cases, the optimal texture length is an outcome of the interplay between pressure gain due to the dimple effect and pressure loss due to side leakage. In short bearings, corresponding to B/L values equal to 1.0 or smaller, a longer textured part is promoted in the case of k=0 (Figure 13(b)), since side leakage in this case is less pronounced, in comparison to converging bearings (Figure 13(d)). As the importance of side leakage diminishes for wide bearings, the trend is reversed for values of B/L equal to 2.0 (Figure 13 (a,c)) and higher.

Evaluation of formulas for texture definition

In Figure 7, the optimal combinations of non-dimensional untextured outlet length, l_{uo}, and relative dimple depth, s, versus convergence ratio, for several B/L ratios, have been illustrated. The approximate formulas of the fitted straight lines presented in Figure 7 are now used to determine the optimal texturing parameters, for sliders of various k and B/L values. Figure 14(a-b) presents the calculated non-dimensional load carrying capacity, W^*, and friction coefficient, f, of textured sliders, for convergence ratios varying from -0.4 to 2; in all cases the geometry has been defined from the fitted formulas presented in Figure 7. It is found that the increasing part of the curves practically coincides with the Pareto fronts of Figure 5. The following observations are made:

- For all B/L values, substantial increase in W^* and decrease in f is obtained, in comparison to smooth bearings, for small and moderate values of convergence ratio. The improvement is marginal at k values higher than approximately 1.4.
- Large values of load carrying capacity and small values of friction coefficient are maintained in a wide range of convergence ratio values. This could substantially decrease uncertainties related to inaccuracies due to manufacturing, especially in bearings for MEMS or micro-turbomachinery applications.

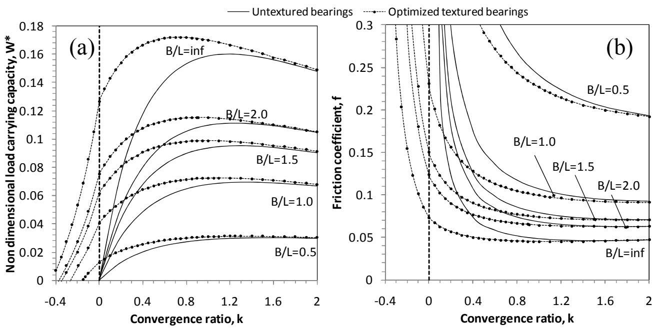

Figure 14. (a) Non-dimensional load carrying capacity, and (b) friction coefficient, vs. convergence ratio, for texture geometries based on the fitted equations presented in Figure 7.

Effects of texture density and number of dimples

The problem formulation of the present optimization study of 3-D bearings has built on the recent results of the 2-D study reported in [19], according to which load carrying capacity is: (a) a continuously increasing function of texture density, ρ_T, and (b) a continuously decreasing function of the number of dimples, N. To check that these dependencies hold in 3-D, we have performed a systematic variation of ρ_T and N, for B/L=1.0. Here, the values of l_{uo} and s are the optimal ones at given k. The resulting load capacity values, presented in Figure 15, verify that: (a) the suggested optimal patterns provide significant load carrying capacity for different values of ρ_T and N, and (b) the trends remain unchanged in 3-D. It is noted that inclusion of parameters ρ_T, and N in the design variables would simply result in optimal step bearings. Instead, a value should be prescribed for each of ρ_T and N, based on strength and wear considerations, respectively.

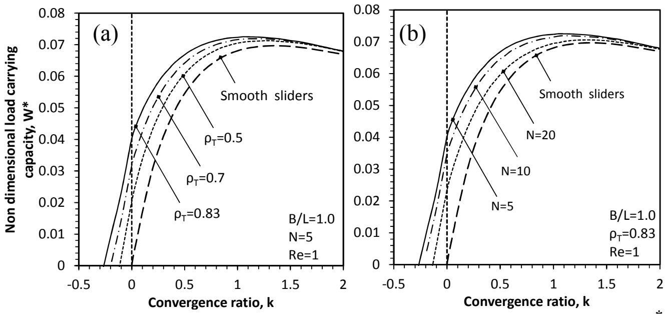

Figure 15. B/L=1.0: non-dimensional load carrying capacity, W^*, vs. convergence ratio, k, for (a) different values of texture density, ρ_T, and (b) different number of dimples, N. Variables l_{uo} and s are derived from the proposed formulas of Figure 7.

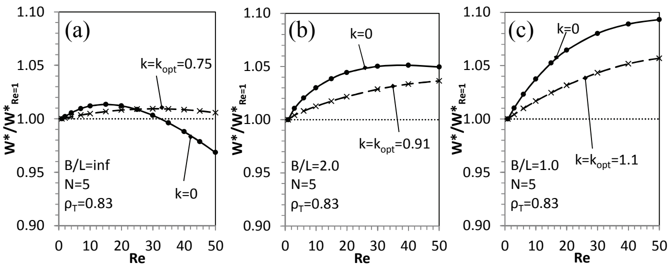

Figure 16. N=5, ρ_T=0.83: normalized non-dimensional load carrying capacity, $W^*/W^*_{Re=1}$, vs. Reynolds number, Re, for different values of convergence ratio, k, for (a) B/L=inf, (b) B/L=2.0, (c) B/L=1.0.

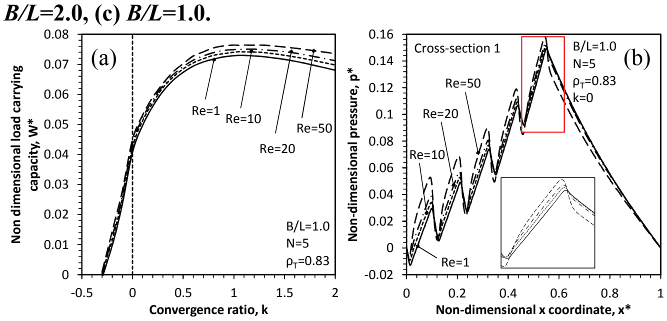

Figure 17. B/L=1.0, N=5, ρ_T=0.83: (a) non-dimensional load carrying capacity, W^*, vs. convergence ratio, k, for different values of Reynolds number, Re. (b) distribution of non-dimensional pressure at the bearing symmetry plane for k=0 for different Re values.

Reynolds number effects

As a final investigation, the dependence of load carrying capacity on Reynolds number, Re, has been considered. Figure 16 presents the non-dimensional load carrying capacity, normalized by the corresponding value at Re=1, as a function of Re; here, the texture patterns are derived from the proposed approximate formulas of Figure 7. In infinitely wide parallel sliders, W^* initially increases with Re, reaches a maximum at Re approximately equal to 15, and subsequently decreases. At increasing convergence ratios or decreasing *B/L* ratios, the increasing trend in W^* is maintained for a wider range of Re. For all cases of Figure 16, the difference in W^*, with respect to Re=1, is less than 10%. In Figure 17(a), for bearings with *B/L*=1.0, W^* is plotted vs. *k* for several Re numbers; an increase of W^* with Re is observed over a wide range of convergence ratio values. The non-dimensional pressure distribution at the symmetry plane of a parallel bearing with *B/L*=1.0, presented in Figure 17(b), reveals that inertia induced effects increase the pressure buildup slope in the dimple areas; the corresponding increased pressure drop at the lands after each dimple is less pronounced at the range of Re under consideration, leading to an overall positive pressure buildup (see also discussions in [11,13]). The overall effect is reversed at Reynolds numbers higher than a critical one; this critical value is a function of the *B/L* ratio, see Figure 16 .

CONCLUSIONS

An optimization approach based on genetic algorithms has been applied to the geometry optimization of 3-D textured micro- thrust bearings, for maximum load carrying capacity. For a number of width-to-length ratios, a large number of texture geometries has been tested, in terms of computing the flow fields, by means of a Navier-Stokes solver. The optimal texturing patterns have been identified for a wide range of bearing convergence ratios. The following conclusions are drawn:

- The introduction of optimal texture patterns improves substantially the bearing load capacity, in comparison to that of smooth sliders, especially at small convergence ratio values. Optimally textured sliders provide increased W^* compared to optimal smooth channels; the increase reaches 7.5% for sliders of infinite width. Large values of load capacity and small values of friction coefficient are maintained over a wide range of convergence ratio values. Substantial pressure buildup is possible even for slightly diverging textured channels.
- The optimal value k_{opt} for textured sliders is a decreasing function of *B/L*. Low-width optimal sliders (*B/L* up to approximately 1.0) provide higher load carrying capacity than corresponding optimal step bearings.
- The proposed approximate formulas can be used to determine the optimal texturing parameters, for sliders of various *B/L* and *k* values. Use of the proposed formulas results in significant increase in load carrying capacity, for a wide range of texture density, ρ_T, number of dimples, *N*, and Reynolds number, Re, values.

ACKNOWLEDGMENT

This work has been partially supported by the EU project MARINELIVE, grant Nr. 264057. This support is gratefully acknowledged.

NOMENCLATURE

Micro- thrust bearing geometry variables (Figure 1a)

B	slider width (m)
B/L	slider width-to-length ratio
H_0, H_1	outlet, inlet height (m)
$H_{\min}$	minimum film thickness (m): $H_{\min} = \min(H_0, H_1)$
k	convergence ratio: $k = (H_1 - H_0)/H_0$
L	slider length (m)
l	non-dimensional slider length: $l = L/H_{\min}$
L_{ui}	untextured inlet length (m)
l_{ui}	non-dimensional untextured inlet length: $l_{ui} = L_{ui}/L$
L_{uo}	untextured outlet length (m)
l_{uo}	non-dimensional untextured outlet length: $l_{uo} = L_{uo}/L$
x^*	non-dimensional *x* coordinate: $x^* = x/L$

Dimple geometry variables (Figure 1b)

H_d	dimple depth (m)
L_c	texture cell length (m): $L_c = L(1 - l_{ui} - l_{uo})/(N + \rho_T - 1)$
L_d	dimple length (m)
N	number of dimples
s	relative dimple depth: $s = H_d/H_{\min}$
ρ_T	texture density: $\rho_T = L_d/L_c$

Physics variables

f	friction coefficient: $f = F_{fr}/W$
F_{fr}, F_p	friction force, vertical pressure force (N)
p	pressure (Pa)
p^*	non-dimensional pressure: $p^* = \frac{p}{\rho U^2} \mathrm{Re} \frac{H_{\min}}{L}$
Re	Reynolds number: $\mathrm{Re} = \rho U H_{\min}/\mu$
U	moving wall velocity (m s^{-1})
u, v, w	streamwise, cross-flow and spanwise fluid velocities (m s^{-1})
$\mathbf{V}$	fluid velocity vector: $\mathbf{V} = u\mathbf{i} + v\mathbf{j} + w\mathrm{k}$
W	absolute value of external bearing force (load carrying capacity) (N)
W^*	non-dimensional load carrying capacity: $W^* = \frac{W}{\mu U B}\left(\frac{H_{\min}}{L}\right)^2$
μ	fluid dynamic viscosity (Pa s)
ρ	fluid density (kg m^{-3})
τ	shear stress (Pa)

REFERENCES

1. Shan, X. C., Zhang, Q. D., Sun, Y. F., and Maeda, R., 2007. "Studies on a Micro Turbine Device with both Journal- and Thrust-Air Bearings". *Microsystem Technol*ogies, **13**, pp. 1501–1508.
2. Nakano, S., Kishibe, T., Inoue, T., and Shiraiwa H., 2009. "An Advanced Microturbine System with Water-Lubricated Bearings".

International Journal of Rotating Machinery, **2009***,* doi:10.1155/2009/718107.

3. Peirs, J., Reynaerts, D., and Verplaetsen, F., 2003. "Development of an axial microturbine for a portable gas turbine generator". *Journal of Micromechanics and Micro*engineering*,* **13,** pp. 190–195.
4. Yang, H., Ratchev, S., Turitto, M., and Segal, J., 2009. "Rapid Manufacturing of Non-Assembly Complex Micro-Devices by Stereolithography". *Tsinghua Science and Technology,* **14**, pp. 164-167.
5. Andharia, P. I., Gupta, J. L., and Deheri, G. M., 2000. "On the Shape of the Lubricant Film for the Optimum Performance of a Longitudinal Rough Slider Bearing". *Industrial Lubrication and Tribology*, **52**(6), pp. 273-276.
6. Tonder, K., 1987. "Effects of Skew Unidirectional Striated Roughness on Hydrodynamic Lubrication". *Wear*, **115**(1-2), pp. 19-30.
7. Etsion, I., Halperin, G., Brizmer, V., and Kligerman, Y., 2004. "Experimental Investigation of Laser Surface Textured Parallel Thrust Bearings". *Tribology Letters,* **17**(2), pp. 295-300.
8. Ozalp, A. A., and Umur, H., 2006. "Optimum Surface Profile Design and Performance Evaluation of Inclined Slider Bearings". *Current Science.* **90**(11), pp. 1480-1491.
9. Pascovici, M. D., Cicone, T., Fillon, M., and Dobrica, M. B., 2009. "Analytical Investigation of a Partially Textured Parallel Slider". *Proceedings of the Institution of Mechanical Engineers, Part J: Journal of Engineering Tribology*, **223**(2), pp. 151-158.
10. Buscaglia, G. C., Ciuperca, I., and Jai, M., 2005. "The Effect of Periodic Textures on the Static Characteristics of Thrust Bearings". *ASME Journal of Tribology*, **127**, pp. 899-902.
11. Dobrica, M. B., and Fillon, M., 2009. "About the Validity of Reynolds Equation and Inertia Effects in Textured Sliders of Infinite Width". *Proceedings of the Institution of Mechanical Engineers, Part J: Journal of Engineering Tribology,* **223**(1), pp. 69-78.
12. Cupillard, S., Cervantes, M. J., and Glavatskih, S., 2008. "Pressure Buildup Mechanism in a Textured Inlet of a Hydrodynamic Contact". *Journal of Tribology*, **130**(2)*,* 21701, pp. 1-10.
13. Arghir, M., Roucou, N., Helene, M., and Frene, J., 2003. "Theoretical analysis of the incompressible laminar flow in a macro-roughness cell". *Journal of tribology,* **125**(2), pp. 309-318.
14. Marian, V. G., Kilian, M., and Scholz, W., 2007. "Theoretical and Experimental Analysis of Partially Textured Thrust Bearing with Square Dimples". *Proceedings of the Institution of Mechanical Engineers, Part J: Journal of Engineering Tribology*, **221**, pp. 771-778.
15. Han, J., Fang, L., Sun, J., and Ge S., 2010. "Hydrodynamic Lubrication of Microdimple Textured Surface Using Three-Dimensional CFD". *Tribology Transactions,* **53**, pp. 860-870.
16. Van Ostayen, R. A. J., Van Beek, A., and Munnig-Schmidt, R. H., 2007. "Film Height Optimization of Hydrodynamic Slider Bearings". In Proceedings of the ASME/STLE International Joint Tribology Conference, IJTC 2007 PART A, pp. 237-239.
17. Buscaglia, G. C., Ausas, R. F., and Jai, M., 2006. "Optimization Tools in the Analysis of Micro-Textured Lubricated Devices". *Inverse Problems in Science and Engineering*, **14**(4), pp. 365-378.
18. Dobrica, M. B., Fillon, M., Pascovici, M. D., and Cicone, T., 2010. "Optimizing Surface Texture for Hydrodynamic Lubricated Contacts Using a Mass-Conserving Numerical Approach". *Proceedings of the Institution of Mechanical Engineers, Part J: Journal of Engineering Tribology*, **224**(8), pp. 737-750.
19. Papadopoulos, C. I., Nikolakopoulos, P. G., and Kaiktsis, L., 2011. "Evolutionary Optimization of Micro- Thrust Bearings with Periodic Partial Trapezoidal Surface Texturing". *Journal of Engineering for Gas Turbines and Power,* **133**, 012301, pp. 1-10.
20. Stachowiak, G. W., and Batchelor, A. W. 2005. "Engineering Tribology", Butterworth and Heinemann, Burlington.
21. Nikolakopoulos, P. G., Papadopoulos, C. I., and Kaiktsis, L., 2010. "Elastohydrodynamic Analysis and Pareto Optimization of Intact, Worn and Misaligned Journal Bearings". *Meccanica,* DOI 10.1007/s11012-010-9319-7.
22. Cahon, S., Melab, N., and Talbi, E. G., 2004. "ParadisEO: A Framework for the Reusable Design of Parallel and Distributed Metaheuristics". *Journal of Heuristics*, **10**(3), pp. 357-380.
23. Deb, K., Pratap, A., Agrawal, S., and Meyarivan, T., 2002. "A Fast and Elitist Multiobjective Genetic Algorithm: NSGA-II". *IEEE Trans*actions on *Evolutionary Computation,* **6**(2), pp. 182-197.
24. Qide Z., 2003. "Fluid Bearing Spindles for Data Storage Devices". Ph.D. Thesis, National University Of Singapore.